AIAA JOURNAL
Vol. 36, No. 2, February 1998

Computational and Experimental Study of Liquid Sheet Emanating from Simplex Fuel Nozzle

S. M. Jeng* and M. A. Jog†
University of Cincinnati, Cincinnati, Ohio 45221-0070
and
M. A. Benjamin‡
Parker Hannifin Corporation, Mentor, Ohio 44060

A computational model for flow in a simplex nozzle has been established to predict the characteristics of the liquid sheet emanating from it. An important aspect of the numerical method is the accurate tracking of the liquid/gas interface. Because the interface geometry is not known a priori, it must be determined as part of the solution. The arbitrary-Lagrangian–Eulerian numerical method with finite volume formulation was employed for this purpose. To validate the computational and numerical modeling, experiments have been conducted on a large-scale nozzle using flow visualization techniques. The gas/liquid interface locations inside the nozzle, as well as just downstream of the orifice, have been determined for a range of mass flow rates and injector geometries. Using these measurements, the liquid film thickness and angle of the liquid sheet has been determined. Comparisons of the computational predictions with the experimental measurements show excellent agreement. Results indicate that the current theoretical correlations based on inviscid flow assumptions underestimate the film thickness and overestimate the spray angle significantly in large scale nozzles. It was found that an increase in the atomizer constant K [$=A_p/(D_m d_o)$] results in decreasing the spray angle and increasing the liquid film thickness, where A_p is the total swirl slot area, D_m is the effective spin chamber diameter, and d_o is the orifice diameter. The discharge coefficient also increases with the atomizer constant.

Nomenclature

A_a	= air core area at orifice exit
A_o	= orifice area
A_p	= total swirl slot area
C_d	= discharge coefficient, $\dot{m}/[A_o\sqrt{(2\rho\Delta p)}]$
D_m	= effective spin chamber diameter, $D_s - d_p$
D_s	= spin chamber diameter
d_o	= orifice diameter
d_p	= swirl slot hydraulic diameter
K	= atomizer constant, $A_p/(D_m d_o)$
l_o	= orifice length
l_p	= swirl slot length
l_s	= spin chamber length
m	= vertex mass
$\dot{m}$	= mass flow rate
p	= pressure
p_∞	= ambient pressure
R_1, R_2	= radii of curvature
r	= radial coordinate
S	= surface of the momentum control volume
t	= time
u	= axial velocity
$\boldsymbol{V}$	= velocity vector
v	= radial velocity
w	= swirl velocity
$\boldsymbol{X}$	= position vector of a node point
x	= axial coordinate
θ	= spray angle
μ	= dynamic viscosity
μ_t	= turbulent dynamic viscosity
ρ	= density
σ	= surface tension

Presented as Paper 97-0796 at the AIAA 35th Aerospace Sciences Meeting, Reno, NV, Jan. 6–9, 1997; received Feb. 18, 1997; revision received Sept. 23, 1997; accepted for publication Oct. 6, 1997.

*Associate Professor, Department of Aerospace Engineering and Engineering Mechanics. Member AIAA.
†Assistant Professor, Department of Mechanical, Industrial, and Nuclear Engineering.
‡Technical Team Leader, Gas Turbine Fuel Systems Division, 9200 Tyler Boulevard. Member AIAA.

Introduction

SIMPLEX atomizers (pressure-swirl atomizers) producing hollow cone fuel sprays are commonly used in air-breathing gas turbine engines because they produce good atomization characteristics and are relatively simple and inexpensive to manufacture. To reduce NO_x emissions, it is critical to design fuel nozzles that can produce sprays with a predetermined droplet size distribution at the desired combustor locations (small Sauter mean diameter and uniform local fuel/air ratios). With the advanced engine programs pushing up the inlet temperature for the combustors, the performance requirements of the nozzles are becoming increasingly tight and demanding. Prediction of the nozzle performance for design and analysis, therefore, is critical to help combustor designers meet the stringent performance requirements.

Current design methods and available correlations for prediction of spray characteristics from a simplex nozzle are outlined by Lefebvre.[1] He provides a detailed review of the experimental and theoretical studies on the flow phenomena in atomizers and spray formation. It is also documented that a change in the geometry of the nozzle can significantly alter its performance. Currently, semiempirical correlations are used to provide guidance in designing simplex nozzles. Studies of flow simulation[2] in a simplex nozzle are very limited in the published literature. The main difficulty in the numerical simulation of flow in a simplex nozzle is the accurate tracking of the interface between the two phases (fuel/air). Several methods of capturing the fuel/air interface have been proposed. Hirt and Nichols[3] have used a volume-of-fluid (VOF) method to track a free surface. In this method the interface is represented in terms of the fraction of the cell volume occupied by the liquid. The accuracy depends on the ability to advect the volume fraction through the grid accurately without numerical smearing. This consideration means that the VOF method can be computationally expensive to get accurate solutions. The gradient method[4] does not define the exact location of the interface within a cell but represents the interface as a continuous

gradient over several cells. Although this method is computationally efficient, the accurate determination of the location of the interface is not possible. The most promising approach for capturing a moving interface is by using a fully Lagrangian formulation.[5] A Lagrangian method can track the interface accurately as the grid moves with the local fluid velocity so that the interface is always located on well-defined cell boundaries. However, a Lagrangian calculation procedure may lead to a highly distorted grid system except for very well-behaved flows. To overcome this difficulty, we have used the arbitrary-Lagrangian–Eulerian (ALE)[6] method in our numerical model. The ALE method combines the accurate Lagrangian tracking of the interface and an Eulerian regridding to avoid a distorted grid. An adaptive grid generation technique[7] is used to body fit the interior grids to the free surface. The algorithms for the body-fitted adaptive grid generation technique and the computational procedure for free surface tracking have been previously validated in the prediction of droplet oscillations and break-up behavior by Deng and Jeng,[8] Deng et al.,[9] Deng and Jeng,[10] and Deng et al.[11] Numerical damping and diffusion were shown to be insignificant in the predictions of droplet dynamics.

Experiments have been conducted using optical methods to measure the thickness and angle of the liquid sheet emanating from a large-scale prototype simplex nozzle. The study consisted of 15 nozzle geometries with four mass flow rates. The large-scale nozzle provides adequate resolution for comparison with the computational results and to validate our model. The predictions of flowfield, liquid sheet thickness, and spray angle by our computational model show excellent agreement with the experimental measurements.

Problem Description

Figure 1a shows a schematic of a simplex nozzle. The liquid enters through the swirl slots, and due to the slot geometry, the liquid has nonzero angular and radial velocity components. The liquid exits from the nozzle in the form of a thin liquid sheet forming a hollow cone. Farther downstream, the sheet becomes unstable and breaks up to form a spray of droplets. Figure 1b shows a typical computational domain used in this study that consists of the flow inside a simplex nozzle and the liquid sheet issuing from the orifice before breakup. For flow involving both gas and liquid phases, a computational model must incorporate the normal stress balance, the shear stress balance, and the no-slip condition at the gas/liquid interface. However, for typical flow conditions in a simplex nozzle, the density and viscosity ratios of liquid to gas (air) are very large. The shear stress acting on the liquid at the gas/liquid interface is very small, and the vorticity generation due to the free surface curvature is also expected to be very small. Therefore, the interface can be treated as an inviscid free surface. As a consequence of this simplification, the flowfield in the gas phase need not be considered. However, the position and geometry of the gas/liquid interface is not known a priori and must be determined as a part of the solution.

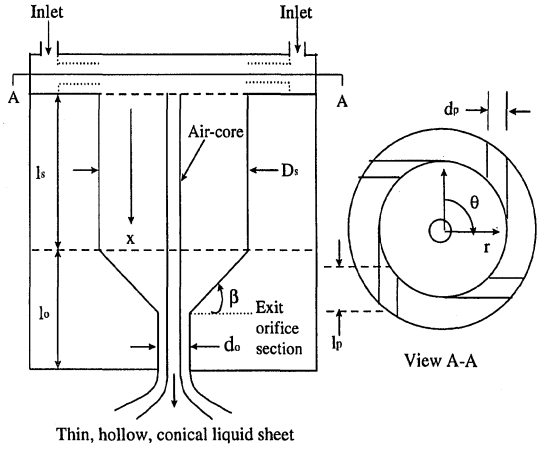

Fig. 1a Typical geometry of a simplex nozzle.

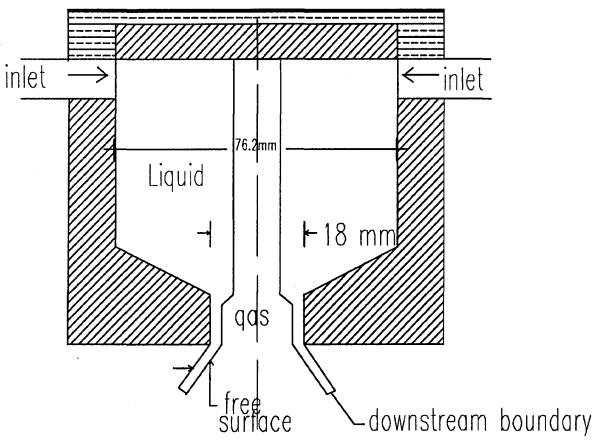

Fig. 1b Computational domain.

Prediction of the flow in the nozzle requires tracking of the gas/liquid interface without any numerical diffusion at the interface. This is accomplished by an ALE numerical method. The ALE method combines the accurate Lagrangian tracking of the interface and an Eulerian regridding to avoid a distorted grid. An adaptive grid generation technique[7] is used to body fit the interior grids to the free surface. The details of the ALE method can be found in Refs. 8 and 9. Only a brief description is provided here.

Computational Model

A computational model based on the ALE method was developed to predict the flow in a simplex nozzle. The flow is considered to be axisymmetric and incompressible. The flowfield is calculated by the solution of the continuity and Navier–Stokes equations. The governing equations can be written in cylindrical coordinates as

$$\frac{\partial(\rho u)}{\partial x}+\frac{1}{r}\frac{\partial(r\rho v)}{\partial r}=0 \tag{1}$$

$$\rho\frac{\partial u}{\partial t}+\rho u\frac{\partial u}{\partial x}+\frac{\rho v}{r}\frac{\partial u}{\partial r}=-\frac{\partial p}{\partial x}+(\mu+\mu_t)\left[\frac{\partial^2 u}{\partial x^2}+\frac{1}{r}\frac{\partial}{\partial r}\left(r\frac{\partial u}{\partial r}\right)\right] \tag{2}$$

$$\rho\frac{\partial v}{\partial t}+\rho u\frac{\partial v}{\partial x}+\frac{\rho v}{r}\frac{\partial v}{\partial r}=-\frac{\partial p}{\partial r}+(\mu+\mu_t)\times\left[\frac{\partial^2 v}{\partial x^2}+\frac{1}{r}\frac{\partial}{\partial r}\left(r\frac{\partial v}{\partial r}\right)\right]+\frac{\rho w^2}{r}-2(\mu+\mu_t)\frac{v}{r} \tag{3}$$

$$\rho\frac{\partial w}{\partial t}+\rho u\frac{\partial w}{\partial x}+\frac{\rho v}{r}\frac{\partial w}{\partial r}=(\mu+\mu_t)\left[\frac{\partial^2 w}{\partial x^2}+\frac{1}{r}\frac{\partial}{\partial r}\left(r\frac{\partial w}{\partial r}\right)\right]-\frac{\rho v w}{r} \tag{4}$$

The mixing length model proposed by Baldwin and Lomax[12] is adopted in this study to calculate the turbulent viscosity at each node point.

Boundary conditions considered in this study are now described. At the swirl chamber inlet, radial and swirl velocity components are specified. To make fruitful comparisons between the axisymmetric computational fluid dynamics (CFD) model that has an annular inlet slot and the experimental configuration that has a finite number of square inlet slots, it is necessary to determine the equivalent axisymmetric inlet conditions for the computational model. This is accomplished by matching the total mass flow rate, angular momentum, and kinetic energy of the liquid at the inlet to the swirl chamber. These conditions are used to determine the inlet slot height and velocity components for the CFD calculations. The radial and the swirl velocity component were assumed to be constant across the inlet slot in the computational model. At the end of the liquid sheet, flow properties were extrapolated from interior grid points by considering first derivatives along a streamline to be zero.

At the gas/liquid interface, the normal stress balance is $p = p_\infty + \sigma(1/R_1+1/R_2)$, where p_∞ is the ambient gas phase pressure, which

is assumed to be constant. The method to calculate the radii of curvature at any point is described in Ref. 8. The velocity gradients of liquid normal to the interface are assumed to be zero because the gas phase shear stress at the interface is small.

Note that from the solution of the governing equations [Eqs. (1–4)] we have calculated the mean flow properties. The fluctuations in the velocity and pressure, as well as the free surface instabilities, have not been evaluated. The preceding governing equations and boundary conditions are discretized by a finite volume technique. A staggered grid is used for pressure and velocity cells to obtain convergent solutions. The ALE method is used with an adaptive grid generation technique. The ALE method comprises two computational steps. In the first step, the computational grid vertices move with the same velocity as that of the fluid. There is no mass exchange among the computational cells. This is the Lagrangian calculation step. A predictor–corrector numerical scheme is used to solve the continuity and the momentum equations. The predictor first calculates the temporary velocity increment for vertex (i, j) for each time step based on a temporary new pressure field p^*:

$$\Delta V_{i,j} = \frac{\Delta t}{m_{i,j}} \oint_S p^* \, dA \tag{5}$$

where S is the surface of the momentum control volume, $m_{i,j}$ the vertex mass, and Δt the time increment. Then the positions of vertices are updated as

$$V^*_{i,j} = V^N_{i,j} + \Delta V^*_{i,j} \tag{6}$$

$$X^*_{i,j} = X^N_{i,j} + V^*_{i,j} \Delta t \tag{7}$$

and the cell mass $m^*_{i,j}$ can be calculated based on the temporary volume. If the updated cell mass $m^*_{i,j}$ does not agree with the cell mass $m_{i,j}$ of the previous time step, the corrector step uses the conjugate-gradient method to find a new pressure field. When the cell mass converges, the velocity and pressure at time $t + \Delta t$ are obtained.

In the second step of the ALE method, a new adaptive grid is generated. A donor–acceptor method is used to calculate the mass and momentum fluxes due to the motion of the new grid vertices from their Lagrangian positions. The velocities at the new grid points are then calculated for time $t + \Delta t$. During the computations, the free surface position moves as computational time proceeds. The steady-state solution is achieved when the normal velocity component at all of the nodes on the interface becomes zero. The free surface position and flowfield within the computational domain are then stored.

Most of the runs were carried out with 61 node points in the axial direction and 21 node points in the radial direction. In the Lagrangian step, the solution was considered to be converged if the maximum relative error in cell mass between two iterations was less than 10^{-7}. A typical run required approximately 35 h on a Pentium-Pro 200 MHz personal computer.

The established computational model has been used to understand the flow physics inside large-scale simplex nozzles. The predicted thicknesses and angles of the liquid sheets emanating from the nozzle are compared next with experimental data for a range of flow rates and different injector geometries.

Experimental Measurements

Typically, simplex fuel nozzles for aircraft engines are very small with orifice diameters on the order of 0.5 mm. Therefore, with current measurement techniques, it is practically impossible to make accurate measurements of the fluid flow properties within these injector bodies, as well as of the spray near the injector. To understand the underlying physics of the flow and to develop precise models, it is necessary to obtain these measurements with sufficiently high resolution. To overcome these difficulties, a large-scale simplex nozzle with a swirl chamber diameter of 76 mm and orifice diameter of 18 mm is used to provide sufficient spatial resolution for accurate observation (Fig. 2). Although the large-scale nozzle data may not directly scale down to predict the performance of conventional scale nozzles, they are very valuable to validate the computational model. The

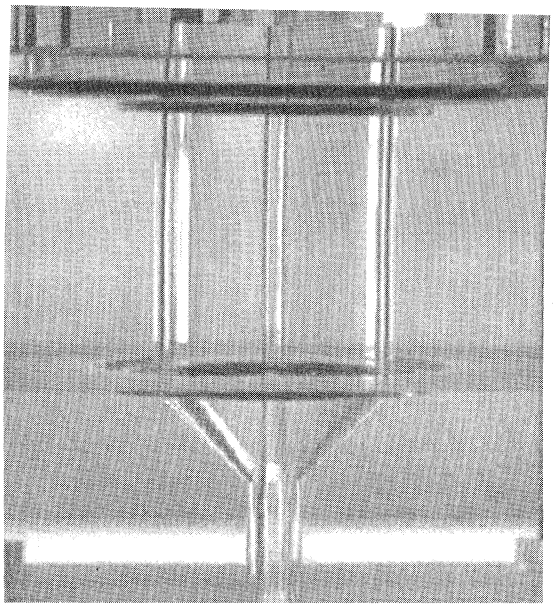

Fig. 2a Assembled simplex nozzle with working fluid.

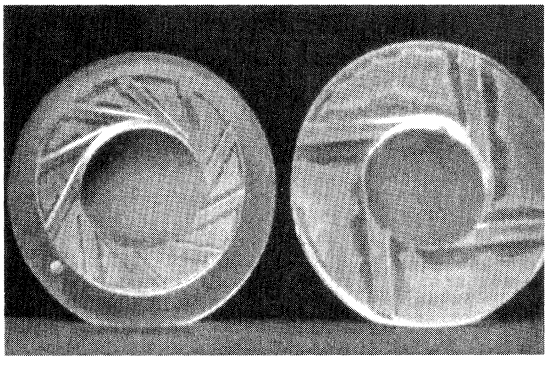

Fig. 2b Two swirlers (10 and 4 slots) used in the study.

body of the large-scale prototype simplex nozzle is made of optical-quality Plexiglas® to accommodate the optically based diagnostic tools. The injector consists of three interchangeable major parts: the swirl slots contained in a housing, straight section before the orifice, and orifice section. These parts are made to be easily changeable to simulate the effects of changing internal passage dimensions on injector performance. Three spin chamber lengths (l_s = 116, 89, and 38 mm) and two orifice section lengths (l_o = 36 and 9 mm) were used.

Water is the working liquid and is injected vertically downward in still air. The test liquid is collected in a baffled tub (with a small down draft produced by a fan) to prevent splashing into the area where measurements are made and then is discharged to a floor drain. Cameras [charge-coupled device (CCD) and still photography] were used to record the instantaneous liquid surface positions. These images were then analyzed to determine the liquid sheet thickness and spray angle. Experiments were conducted for injector pressure drops from 69 to 345 kPa and water flow rates from 0.95 to 2.2 kg/s. Typical images of the flow in the near nozzle section and the spray section are shown in Fig. 3. It is clear that an air core forms at the center of injector body, and the core size increases as the liquid progresses through the nozzle. The liquid/air interface positions are clearly identified in these images, and the liquid film thickness and spray angles can be measured. These measurements are corrected for optical distortion due to the differences in index of refraction of air, water, and Plexiglas.[13] The maximum experimental uncertainty in the discharge coefficient based on the flow and pressure measurements is 2%. The maximum uncertainty in the spray angle determination is estimated as 2 deg, and that in film thickness is less than 15%.

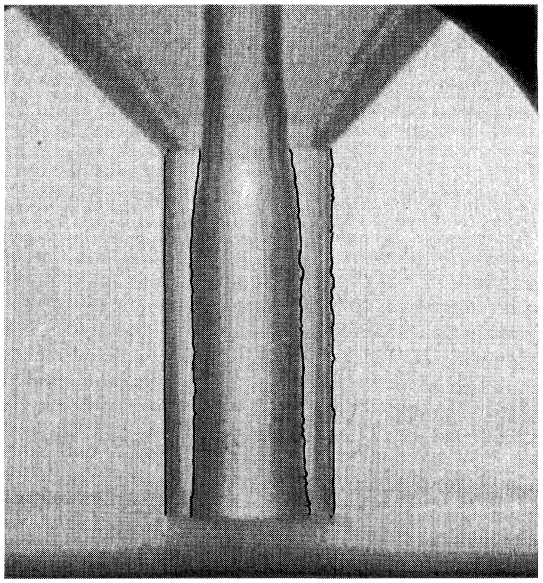

a) Near nozzle section (CCD image)

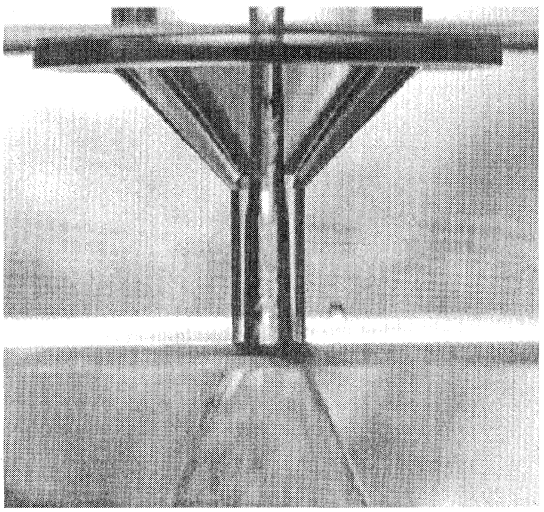

b) Spray section (35-mm photograph)

Fig. 3 Photographs of simplex nozzle flow.

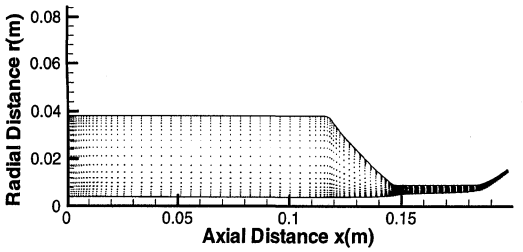

a) Velocity vectors

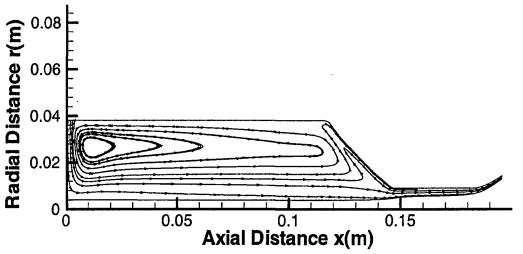

b) Streamlines

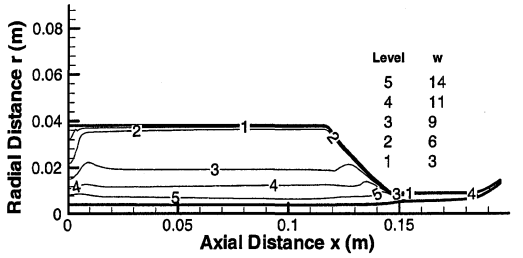

c) Swirl velocity contour

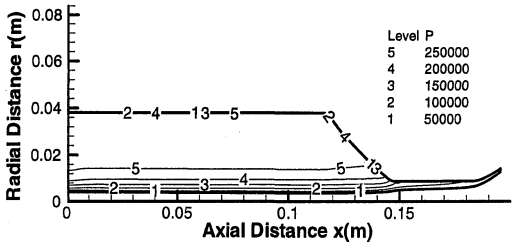

d) Static pressure contours

Fig. 4 Calculated flowfield of simplex nozzle (swirl velocity values in meter per second and pressure in newton per square meter).

Results and Discussion

A parametric study using the developed CFD code was conducted. The injector geometry used for the study is the same as shown in Fig. 1b. The inlet radial velocity was varied from 1.5 to 5.5 m/s and the swirl velocity from 1.5 to 5.5 m/s to simulate the experimental conditions. The Reynolds number, based on the average axial velocity at the orifice exit and the orifice diameter, varied from 2.7×10^5 to 3.5×10^5. Detailed results of a CFD test case are shown in Figs. 4 and 5. Note that the results are obtained for the mean velocity and mean pressure at any given location. The small fluctuations due to turbulence in the velocities and the pressure were not calculated. The liquid/air interface shape shown in Figs. 4 and 5. is consistent with the experimental results shown in Figs. 3a and 3b. The boundary of the air core inside the swirl chamber is straight with a diameter somewhat smaller than that of the orifice. At the orifice entrance, the air core diameter increases abruptly. Figures 4a and 4b show the velocity vector and the streamlines for the flow for a flow rate of 1.5 kg/s. The majority of the fluid flows to the free surface along the top wall of the swirl chamber and then is convected to the orifice along the free surface. A recirculating zone occupies a large portion of the swirl chamber.

The liquid angular velocity within the swirl chamber was found to be relatively uniform in the axial direction, but it decreased in the radial direction, as shown in Fig. 4c. This behavior is consistent with the principle of conservation of angular momentum. Figure 4d shows the pressure variation in the nozzle. The static pressure within the swirl chamber is primarily generated to counterbalance the centrifugal forces of the swirling flow. Because the swirling velocity is quite uniform in the axial direction, the static pressure is also found to be quite uniform in the axial direction.

The velocity vectors and swirling velocity contours of the liquid in the orifice region are shown in Figs. 5a and 5b, respectively. The orifice lip is located at $x = 0.184$ m, from which the liquid sheet spreads out at an angle due to the centrifugal force and forms a hollow cone. The axial velocity distribution and the liquid sheet thickness within the orifice are relatively uniform, and at the orifice exit the liquid sheet thins significantly. As the liquid sheet spreads out downstream, the thickness (normal to the free surface) continues to decrease, but the velocity in the direction of the liquid sheet does not change significantly.

Figure 6 shows the properties of the liquid sheet emanating from the orifice as a function of axial distance. The axial distance is referenced from the orifice exit. Figure 6a shows the mean radial position and thickness of the liquid sheet. From the slope of the radial position, the liquid sheet spreading angle can be calculated. As the liquid sheet moves downstream, the spreading angle increases quickly to a fixed angle (spray angle). For the case shown here, the spreading angle becomes constant over an axial distance of about 4 mm. The calculated liquid sheet thickness decreases nearly linearly as the

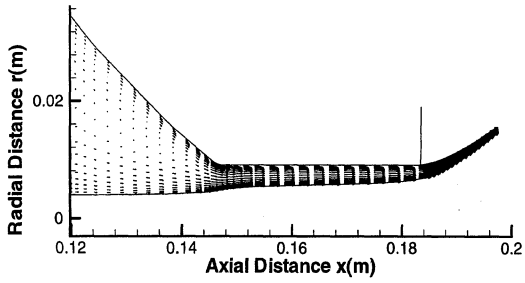

a) Velocity vectors

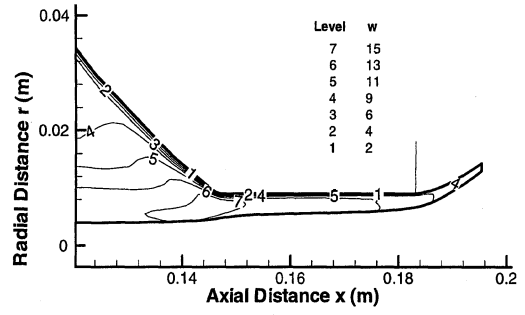

b) Swirling velocity contours

Fig. 5 Calculated flowfield near the nozzle (w in meters per second).

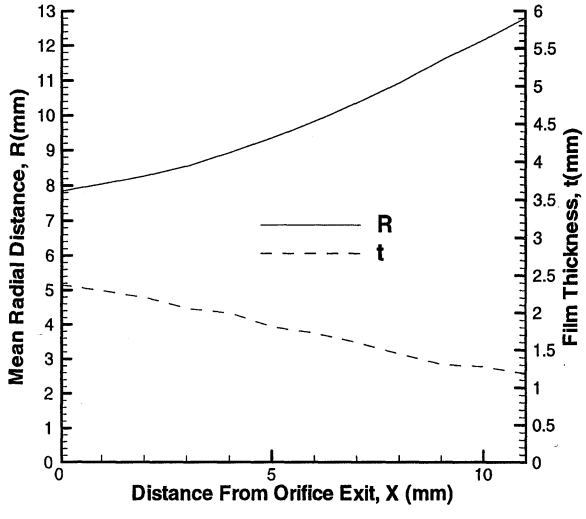

a) Mean radial positions and thickness

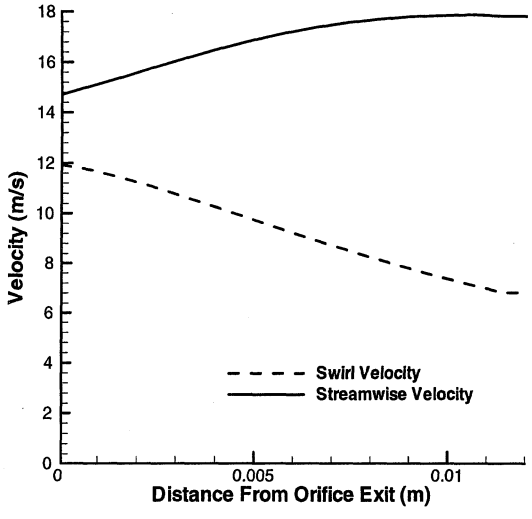

b) Mean swirling and streamwise velocity

Fig. 6 Calculated properties of liquid sheet.

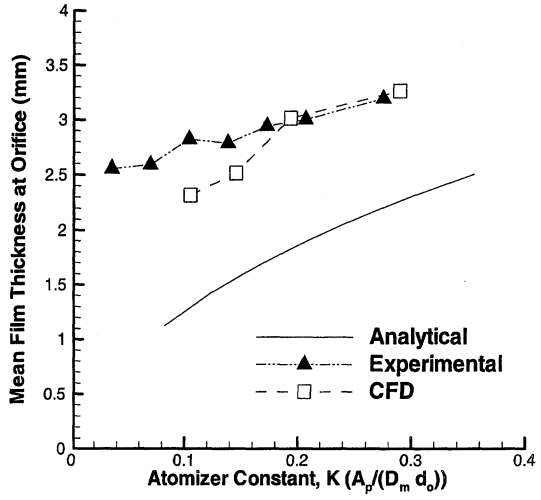

a) Mean liquid sheet thickness at orifice

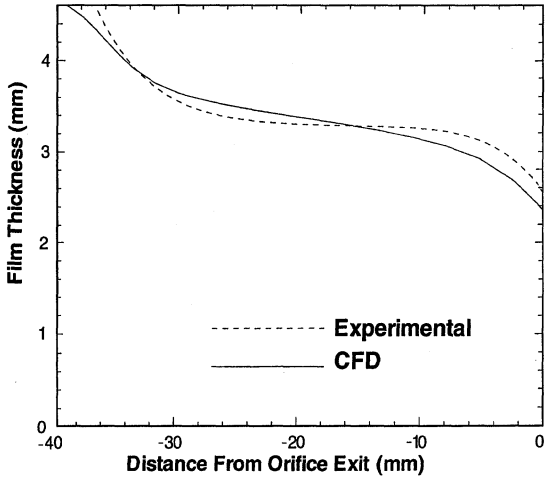

b) Profile of the liquid/gas interface

Fig. 7 Liquid sheet (within nozzle) comparison.

liquid moves downstream. Figure 6b shows the mean streamwise liquid velocity along the liquid sheet direction and swirl velocity as a function of axial distance from the orifice exit. As the liquid sheet spreads out from the orifice, it becomes thinner with higher mean streamwise velocity and lower mean swirl velocity. This behavior is due to the conservation of angular momentum in the liquid sheet.

A comparison of CFD calculations, experimental results, and analytical solutions are shown in Figs. 7–9. The analytical solutions are based on the theory of Giffen and Muraszew[14] and of Rizk and Lefebvre.[15] The theoretical development used to obtain the analytical solutions by Giffen and Muraszew is based on the assumptions of ideal fluid flow with the maximum possible discharge coefficient through the orifice. The derived solutions (discharge coefficient, nondimensionalized film thickness, and spray angle) are only a function of the ratio of axial/swirl momentum flux at the orifice exit, which is linearly related to the nondimensionalized simplex nozzle geometry by the atomizer constant. The current large-scale simplex nozzle experiments show that the mass flow rate (directly related to Reynolds number) and other injector geometries have secondary effects on the liquid sheet characteristics. In the following discussions, K is used to indicate the flow geometry.

Comparison of the film thickness in the orifice is shown in Fig. 7. The analytical film thickness is obtained using the following expression[15]:

$$t = 3.66\left(\frac{d_o \dot{m} \mu}{\rho \Delta p}\right)^{0.25} \tag{8}$$

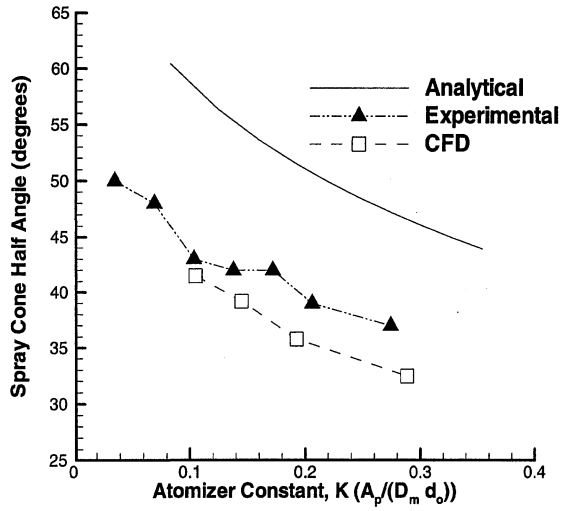

a) Spray angle

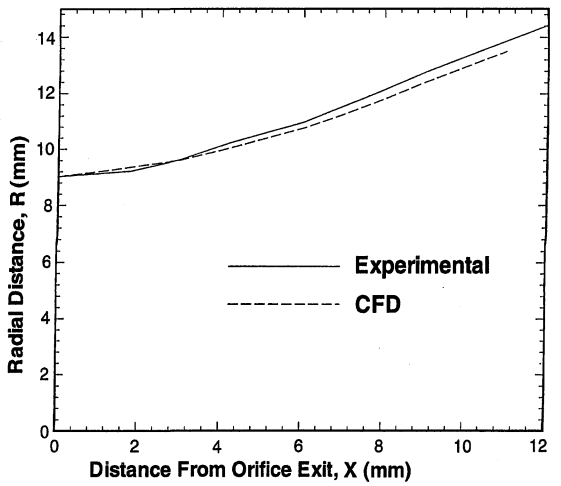

b) Liquid sheet outer suface profile

Fig. 8 Liquid sheet (downstream of orifice) comparison.

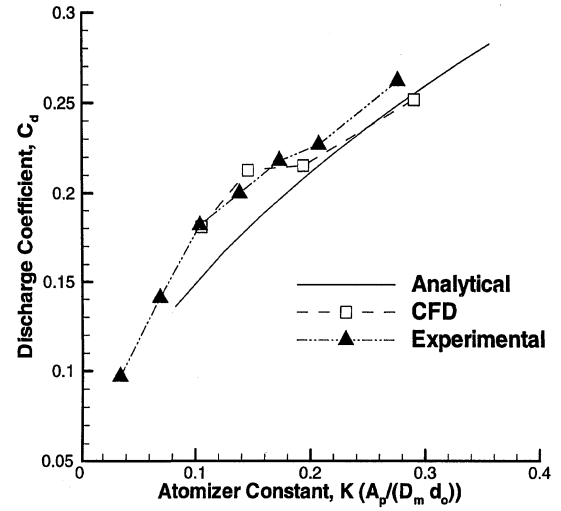

Fig. 9 Variation of discharge coefficient with atomizer constant.

Figure 7a compares the mean liquid film thickness at the orifice exit for a range of atomizer constants. Figure 7b compares the position of the liquid/gas interface as a function of axial distance. Both the CFD and analytical model correctly predict the trend of liquid film thickness as a function of atomizer constant. The CFD calculations agree very well with the experimental results for both the profile of the liquid/gas interface and the mean liquid sheet thickness at the orifice exit for different atomizer constants. However, the analytical model provides only the mean liquid sheet thickness at the orifice exit and underestimates the experimental results significantly. A comparison of film thickness predictions using several semiempirical correlations with the present experimental data is provided in Ref. 16.

Figure 8 shows the spray angles and liquid sheet outer edge position downstream of the orifice exit. An expression provided by Giffen and Muraszew[14] is used to determine the spray angle analytically:

$$\sin\theta = \frac{(\pi/2)(1 - A_a/A_o)^{1.5}}{K(1 + \sqrt{A_a/A_o})(1 + A_a/A_o)^{0.5}} \tag{9}$$

The spray angles of both the CFD and experimental results were taken from the slopes of the outer edge of the liquid sheet at the end of the computational domain. For a given mass flow rate, a reduction in the inlet swirl slot area corresponds to a decrease in the atomizer constant. A reduction in A_p increases the swirl inside the spin chamber and causes the spray angle to increase because of a larger centrifugal force. The CFD and experiments agree well for spray angles, whereas the analytical solutions overestimate them significantly. Figure 9 shows the variation of discharge coefficient as a function of atomizer constant. The following analytical expression for the discharge coefficient[15] is used for comparison with the experimental and the computational results:

$$C_d = 0.35K^{0.5}(D_s/d_o)^{0.25} \tag{10}$$

It is seen from Fig. 9 that the discharge coefficient increases as the axial/swirl momentum ratio increases. Both the CFD and the analytical model correctly predict this trend and agree well with experimental data.

Conclusions

A computational model to predict the flow in a simplex nozzle has been established, and experiments were conducted on a large-scale nozzle using optical methods. A comparison of experimental and computational results shows that the developed CFD model based on the ALE method can accurately predict the flow in a simplex nozzle. Results indicate that the current theoretical correlations based on inviscid flow assumptions underestimate the film thickness and overestimate the spray angle significantly in the large-scale nozzles. It was found that an increase in the atomizer constant results in decreasing the spray angle and increasing the liquid film thickness. The discharge coefficient also increases with the atomizer constant.

Acknowledgments

This work was supported by the Parker Hannifin Corporation, the Ohio Aerospace Institute under Grant CCRP-95-006, and NASA under Grant NAG3-1987. The authors would like to thank D. Holtzclaw, R. Dimicco, and A. Opalski for substantial help in the experiments and T. Sakman for reducing the computational data and analytical calculations.

References

[1]Lefebvre, A. H., *Atomization and Sprays*, Hemisphere, New York, 1989, Chap. 5.

[2]Ritz, N. K., and Chin, J. S., "Comprehensive Fuel Nozzle Model," AIAA Paper 94-3278, June 1994.

[3]Hirt, C. W., and Nichols, B. D., "Volume of Fluid (VOF) Method for the Dynamics of Free Boundaries," *Journal of Computational Physics*, Vol. 39, No. 2, 1981, pp. 201–225.

[4]Deng, Z. T., "Numerical Investigation of Non-Spherical Droplet Dynamics in Viscous Convective Flows," Ph.D. Thesis, Dept. of Aerospace Engineering and Mechanical Engineering, Univ. of Tennessee, Knoxville, TN, Dec. 1991.

[5]Oran, E. S., and Boris, J. P., *Numerical Simulation of Reactive Flow*, Elsevier, New York, 1987, pp. 358–391.

[6]Hirt, C. W., Amsden, A. A., and Cook, J. L., "An Arbitrary Lagrangian–Eulerian Computing Method for All Flow Speeds," *Journal of Computational Physics*, Vol. 14, No. 3, 1974, pp. 227–253.

[7]Thompson, J. F., Warsi, Z. U. A., and Martin, C. W., "Boundary Fitted Coordinate System for Numerical Solution of Partial Differential Equations—A Review," *Journal of Computational Physics*, Vol. 47, No. 1, 1982, pp. 1–108.

[8]Deng, Z. T., and Jeng, S. M., "Numerical Simulation of Droplet Deformation in Convective Flow," *AIAA Journal*, Vol. 30, No. 5, 1992, pp. 1290–1297.

[9]Deng, Z. T., Litchford, R. J., and Jeng, S. M., "Two-Dimensional Simulation of Droplet Evaporation at High Pressure," AIAA Paper 92-3122, July 1992.

[10]Deng, Z. T., and Jeng, S. M., "Numerical Simulation of Non-Spherical Droplet Evaporation in Convective Flows," AIAA Paper 91-2308, June 1991.

[11]Deng, Z. T., Liaw, G., Chou, L., and Jeng, S. M., "Numerical Simulation of Thermocapillary Bubble Migration with Large Deformation," *Proceedings of the 1993 ASME Summer Meeting*, Vol. H0805, American Society of Mechanical Engineers, New York, 1993, pp. 87–94.

[12]Baldwin, B., and Lomax, H., "Thin Layer Approximation and Algebraic Model for Separated Turbulent Flow," AIAA Paper 78-0257, Jan. 1978.

[13]Vikram, C. S., *Particle Field Holography*, Cambridge Univ. Press, Cambridge, England, UK, 1992, Chap. 7.

[14]Giffen, E., and Muraszew, A., *The Atomization of Liquid Fuels*, Wiley, New York, 1953, Chap. 4.

[15]Rizk, N. K., and Lefebvre, A. H., "Internal Flow Characteristics of Simplex Swirl Atomizers," *Journal of Propulsion and Power*, Vol. 1, No. 3, 1985, pp. 193–199.

[16]Benjamin, M. A., Jeng, S. M., and Jog, M. A., "Comparison of Simplex Atomizer Correlations with Detailed CFD and Experimental Data," *Proceedings of the 10th Annual Conference on Liquid Atomization and Spray Systems*, Inst. for Liquid Atomization and Spray Systems-Americas, Irvine, CA, 1997, pp. 45–49.

G. M. Faeth
Associate Editor